Int. J. Rock Mech. Min. Sci. & Geomech. Abstr. Vol. 26, No. 3/4, pp. 211–219, 1989
Printed in Great Britain.

0148-9062/89 $3.00 + 0.00

Stress Control of Seismicity Patterns Observed During Hydraulic Fracturing Experiments at the Fenton Hill Hot Dry Rock Geothermal Energy Site, New Mexico

M. C. FEHLER†

Seismicity accompanying hydraulic injections into granitic rock is often diffuse rather than falling along a single plane. This diffuse zone of seismicity cannot be attributed to systematic errors in locations of the events. A new scheme for determining orientations and locations of planes along which the micro-earthquakes occurred was recently developed. The basic assumption of the method, called the three-point method, is that many of the events fall along well-defined planes; these planes are often difficult to identify visually in the data because planes of many orientations are present. The method has been applied to four hydraulic fracturing experiments conducted at Fenton Hill as part of a hot dry rock geothermal energy project. While multiple planes are found for each experiment, one plane is common to all experiments. The ratio of shear to normal stress along planes of all orientations is calculated using a best estimate of the current stress state at Fenton Hill. The plane common to all experiments has the highest ratio of shear to normal stress acting along it, so it is the plane most likely to slip. The other planes found by the three-point method all have orientations with respect to current principal stresses that are favourable for slip to occur along pre-existing planes of weakness. These results are consistent with the assertion that the rock contains pre-existing joints which slip when the effective stress is reduced by the increased pore fluid pressure accompanying the hydraulic injection. Micro-earthquakes occur along those planes that are favourably aligned with respect to the current stress field.

INTRODUCTION

Seismic monitoring of hydraulic fracturing has been carried out at Fenton Hill by the Los Alamos Hot Dry Rock Group over a period of 12 yr [1–6]. This work has been undertaken with the implicit assumption that the occurrence of seismicity is a direct result of fluid penetration into the rock [7, 8]. Since a hot dry rock geothermal system can only be constructed by connecting two wellbores to a fracture system through which water can flow, there has been continued interest by hot dry rock programs in increasing our understanding of the seismicity accompanying hydraulic fracturing so that the induced fracture system can be delineated.

One major conclusion from the seismic studies is that a majority of the seismic events are shear, not tensile, as proven by their well-constrained fault plane solutions [5, 9–11]. Some exceptions occur, as have been noted by Bame and Fehler [12] and Majer and Doe [13], where long period microearthquakes similar in character to those observed at volcanoes have been observed [14, 15]. These long period events have been interpreted as being the seismic signals from tensile fracturing [12, 14]. Very few long period events accompany the injections and they have been found to occur only during the early stages of the injection when fluid pressures are high enough near the injection point to cause tensile failure. Shear events may occur in close proximity to tensile failure or, alternatively, they may occur at locations where the fluid pressure is not sufficient to cause jacking of the rock but is sufficient to reduce the effective stress to allow shear to occur. Recently, Murphy and Fehler [8], following on the work of Cundall and Marti [16] analyzed the seismicity at Fenton Hill and concluded that the seismicity occurs along pre-existing

†Los Alamos National Laboratory, P.O. Box 1663, MS D443, Los Alamos, NM 87544, U.S.A.

surfaces of weakness in the rock, or joints, that are favourably oriented with respect to the *in situ* stress field to allow shear slip. Murphy and Fehler argued that water flows along these planes after the shear has occurred, since some increase in permeability along the failure plane must accompany the shear slip due to the surface roughness of the joint [17]. If this model is correct, it is desirable to determine where these planes exist in the potential hot dry rock reservoir so that pre-existing fluid flow paths can be taken advantage of to create a fluid flow/heat extraction loop through the reservoir.

Seismicity observed at Fenton Hill has been observed to be diffuse in nature [5, 18], occurring throughout a volume rather than along a single plane as might be expected if fluid were confined to a single tensile fracture. The width of the seismic zone cannot be explained by errors in locations [18]. Recently, Fehler *et al.* [11] developed a method called the three point method, for analyzing sets of seismic locations to determine locations and orientations of discrete planes along which many of the microearthquakes occurred. They applied this method to data accompanying a massive hydraulic fracturing operation carried out at Fenton Hill and found five planes along which slip occurred. Two of the planes determined from the microearthquake locations were parallel to nodal planes of fault plane solutions for many of the microearthquakes. In addition, these planes intersected wellbores in locations where other data indicate the presence of major fracture zones [11]. These correlations between seismically determined planes and other data provide confirmation of the results obtained by the three-point method.

Our hypothesis that the planes along which microearthquakes occur are pre-existing joints that slip in response to the changes in the effective stress due to increased pore fluid pressure leads to the conclusion that the planes must be oriented so that the shear stress along these planes is large relative to that on planes with other orientations. To investigate the relation between the planes defined by the three-point method and estimates of *in situ* stress field, we applied the three-point method to microearthquake locations accompanying four large hydraulic injections carried out at Fenton Hill. The orientations of planes found by the method will be compared with our best estimate of the stress field at Fenton Hill and it will be shown that the planes defined by the three-point method are those with the greatest shear stress acting upon them.

THREE-POINT METHOD

The method is described in detail elsewhere [11] so only a brief synopsis will be given here. The method is an extension to three dimensions of a procedure outlined by Lutz [19] for finding lineaments in 2-D surfical geological data. The method is based on the observation that every combination of three microearthquake locations defines a plane. We begin by calculating the strike and dip of the plane made out of every possible combination of three microearthquake locations within a data set from a single hydraulic fracturing experiment. One intuitive way to find the orientation of any plane along which many microearthquakes occurred would be to separate all of the planes defined by combinations of three locations into "bins" corresponding to ranges of similar orientations, and to then identify which bin has the largest number of planes. This technique would produce a biased result due to the shape of the region in which the microearthquakes occur. This bias was discussed for a 2-D case by Lutz [19]. The bias caused by the shape of the region in which the microearthquakes fall can be eliminated by normalizing the number of combinations in each bin by the number of combinations in each bin found for synthetic sets of location data. These synthetic locations are uniformly but randomly distributed throughout the zone in which the actual microearthquakes were found to occur. In this way, an unbiased estimate of the orientation of planes along which microearthquakes fall is obtained and by comparison with many sets of synthetic locations, a statistical estimate of the reliability of the result can be made.

Once the orientation of a plane is determined, the absolute location of the plane can be found by counting how many times, T_j, a particular microearthquake j combines with other microearthquakes to form planes with the preferred orientation. The earthquakes that have the largest value of T_j are those that fall along the plane. By plotting the locations of these events, we find the location of the plane defined by the data.

The method can be successively applied to a given dataset to find planes of differing orientations and locations. By removing those earthquakes that were found to define the plane, we eliminate the preference for that orientation in a subsequent application. In this manner further planes can be obtained from the data.

The method has been extensively tested on synthetic data. In a typical test, synthetic locations that fall along a pre-determined plane were generated and supplemented with points that fall randomly but uniformly in a zone surrounding the plane. The three-point method was applied and the plane located. The points that fell along the plane were subsequently perturbed away from the plane to represent errors in microearthquake locations. The ability of the three-point method to locate the plane in the presence of this locational noise was then investigated to determine how much error could be added to the locations that originally fell along the plane before the method was unable to resolve the plane. Figure 1 shows an example of such a test. The test data consist of 200 synthetic locations that fall inside a box of dimensions $200 \times 200 \times 400$ m, with the long axis oriented north–south. Twenty-five of the locations were placed along the plane and subsequently perturbed in random directions by an average of 20 m to represent errors in locations. The locations are drawn in vertical cross section oriented perpendicular to the strike of the plane so that the line represents the location of the plane defined by the unperturbed data. The method was

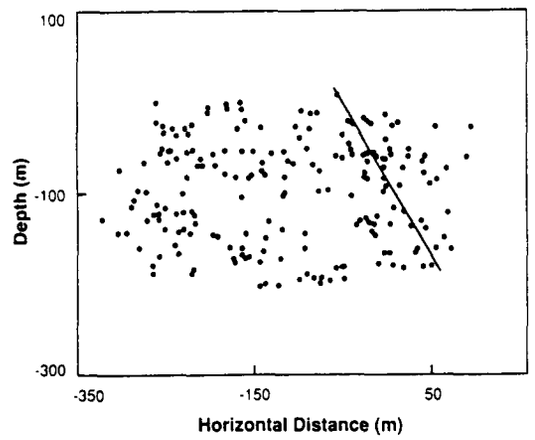

Fig. 1. Vertical cross section showing locations used to test the three-point method. Twenty-five locations were chosen to fall randomly along one plane and 175 locations were chosen to fall randomly throughout a rectangular box of dimensions 400 × 200 × 200 m with the long axis north-south. The locations along the plane were moved in random directions by an average of 20 m to represent errors in microearthquake locations. The plane strikes N60°E and dips 60°E. The view is towards 60°E, parallel to the plane. The points that fall along the plane are connected by a line.

successful in determining the location of the plane in these data even though the plane could not be picked out by eye from examination of location plots. Other tests and examples of applying the method to real data can be found in [11].

DATA COLLECTION AND ANALYSIS

During hydraulic fracturing experiments, seismic data are collected using both surface and downhole seismic stations. Figure 2 is a map showing the locations of the Fenton Hill site and the seismic stations used to monitor seismicity. Stations PC-1, PC-2, GT-1 and EE-1 comprise the downhole seismic network. The remaining stations shown consist of surface sensors. Due to the presence of approx. 700 m of highly attenuating sediments and tuff at the surface in the vicinity of Fenton

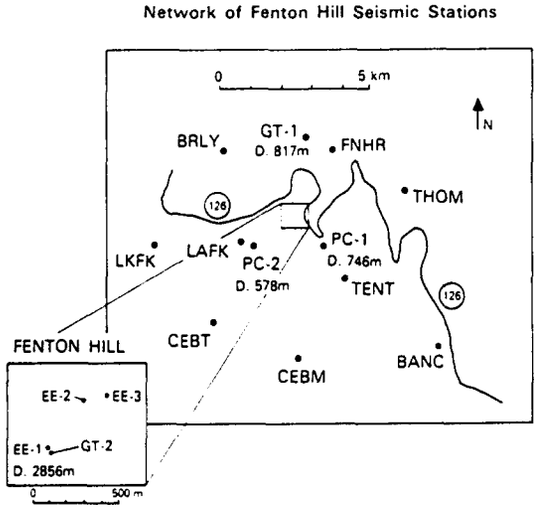

Fig. 2. Map showing locations of the seismic monitoring network in the vicinity of the Fenton Hill hot dry rock site. Stations EE-1, PC-1 PC-2 and GT-1 are subsurface stations. The remaining stations are all located on the surface.

Hill, the surface stations record only the largest events. Since signals recorded at these stations consist of frequencies below 100 Hz, we cannot measure arrival times at these stations precisely enough to determine reliable locations from these data. The downhole sensors, while not all located within the Precambrian granite rock into which we inject water, record frequencies as high as 1 kHz so that arrival times can be determined to within 1 msec. With this precision in arrival times, event locations can be determined to a precision of 20 m. Details are given by House [18]. The surface network is used for environmental monitoring in the event of a large earthquake. Data from these sensors can be analyzed to determine fault plane solutions of the larger (up to $M_L = 1.0$) events.

Data from the downhole seismic sensors are transmitted directly over wires or by radio to a central recording site where both analogue and digital recording are carried out. Analogue recordings are made for archival purposes. Digital data are acquired by a UNIX-based digital data aquisition system. Data are digitized at software selectable rates, typically 500 samples/sec for the surface network data, 5000 samples/sec for all borehole data and 50,000 samples/sec for close in borehole data such as that from station EE-1 (Fig. 2). The system performs event detection on the data from the downhole stations and stores data from all channels when an event is detected. The system has software-selectable pre-event memory so that first arrivals from all stations are stored. The system is capable of storing events at a rate as high as 1/sec. Of the data to be discussed in this paper, only that from experiment 2066 was collected using this system.

Data for experiments 2032, 2042 and 2061, discussed below, were collected using our "old" data acquisition scheme which detected events using a Schmidt trigger operating on data from the sensor in EE-1. This system was capable of storing a limited quantity of data for each event and could store data at a rate of only one event/min. We are currently reprocessing data from experiment 2032 using the UNIX-based system by redigitizing events from analogue tapes to study a larger sample of the events that accompanied this, our largest hydraulic injection to date.

EVENT LOCATIONS

Data from four experiments have been analyzed using the three-point method. Table 1 lists relevant information about each experiment. Figures 3–6 show the locations of microseismic events accompanying each injection. During the time that experiments 2032 and 2042 were carried out, wellbores EE-2 and EE-3 existed as shown in Figs 3 and 4. Since no hydraulic connection was made between the two wellbores by these two injections, wellbore EE-3 was subsequently deviated from its original trajectory as shown in Figs 5 and 6. This wellbore is referred to as EE-3a. During this redrilling phase, numerous hydraulic injections were carried out, of which 2061 and 2066 were two. Experiments 2061 and

Table 1. Hydraulic injections

Experiment No.	Date	Depth to top of injection zone[1]	Wellbore	Volume injected (m^3)	Av. pumping (m^3 sec)	No. of microearthquakes located[2]
2032	6 12 83–9 12 83	3463	EE-2	21,600	0.10	844
2042	15 5 84–19 5 84	3344	EE-3	7600	0.02	946
2061	29 6 85–2 7 85	3766	EE-3a	5600	0.02	1021
2066	30 1 86–1 2 86	3706	EE-3a	4400	0.02	1962

[1]Depths are listed as m below an elevation of 8700 ft above mean sea level.
[2]Reliable locations.

2066 were carried out deep in the EE-3a wellbore and did not result in hydraulic communication wellbores EE-3a and EE-2. Two injections, carried out in shallower portions of the EE-3a wellbore, did result in hydraulic communication between the two wellbores. These experiments, called 2052 and 2062, were also accompanied by seismicity. Only four locatable events were recorded during experiment 2052. Many seismic events accompanied experiment 2062 and these data are currently being re-analyzed.

Locations of microearthquakes accompanying two injections, experiments 2042 and 2061, demonstrate that seismicity grew generally downward from the injection points as shown in Figs 4 and 5. This downward migration of event locations was particularly evident during the later periods of the injections. This downward migration of event locations is consistent with results obtained by the British Hot Dry Rock Project as reported by Pine and Batchelor [20]. They interpreted the downward migration of shear type microearthquakes as being due to an increased shear acting along preexisting joints, caused by differences in the gradients in principal stresses with depth.

Locations of seismicity accompanying experiment 2032, shown in Fig. 3, occur in all directions from the injection point and showed no clear migration of event locations with time. Experiment 2066 (Fig. 6) was carried out in transitional zone in EE-2 between the deeper region where 2061 was carried out and the shallower zone of experiment 2032.

APPLICATION OF THE THREE POINT METHOD

The three-point method was applied to locations of microseismic events determined for each of the four experiments listed in Table 1. Each data set was treated independently for two reasons. First, we estimate that the precision in the relative locations of events in a single experiment is 20 m. The relative error is larger when comparing events from differing experiments. The larger error in relative event locations between experiments arises because of differences in stations locations used to

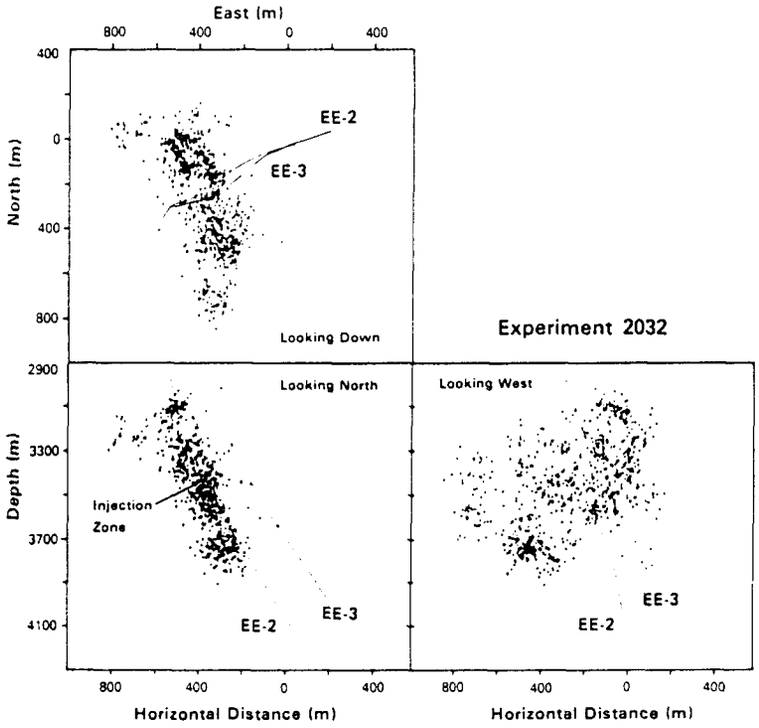

Fig. 3. Three orthogonal views showing locations of actual events accompanying experiment 2032. Upper left: epicenter plot. Lower left: vertical cross section projected onto an east–west plane. Lower right: vertical cross section projected onto a north–south plane. There is no vertical exaggeration in the figures. The trajectory of wellbore EE-2, the injection wellbore, and EE-3 are shown. The injection interval in wellbore EE-2 is labelled.

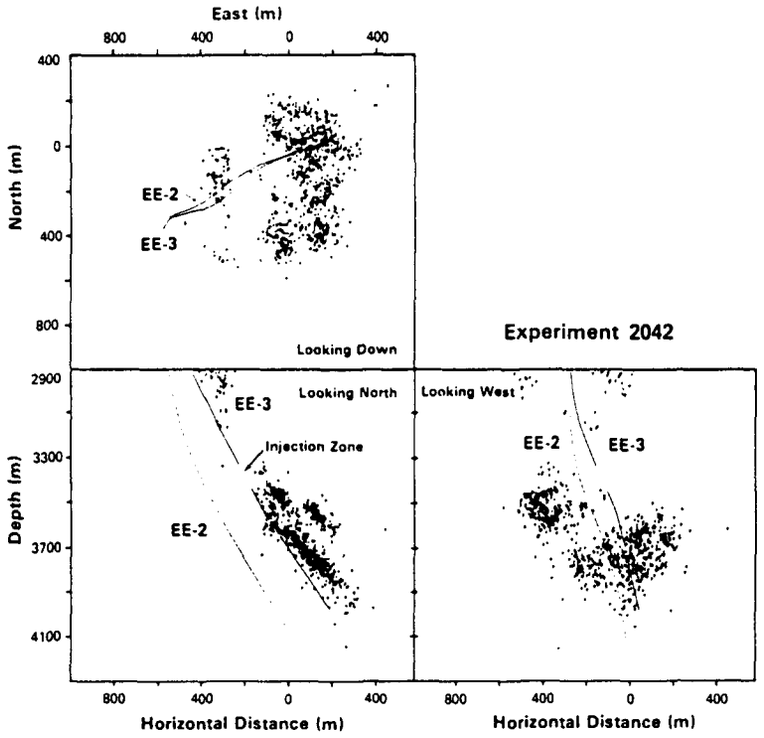

Fig. 4. Three orthogonal views showing locations of microseismic events accompanying experiment 2042. Views are the same as in Fig. 3. Water was injected into wellbore EE-3 in this experiment. The injection interval is labelled in the figure.

record data for various experiments. The second reason for treating each experiment independently is that the amount of computer time required to analyze one dataset increases dramatically as the number of events analyzed increases.

Table 2 lists the orientations of planes found for each experiment. The orientations are listed in the order in which they were determined by the three-point method. In applying the method, events that were found to lie along a plane were removed from the dataset and the method reapplied. In this way, multiple planes along which the microearthquakes fall can be determined. Also listed in Table 2 is the depth of the centre of each plane. This depth is the average depth of the locations of all the

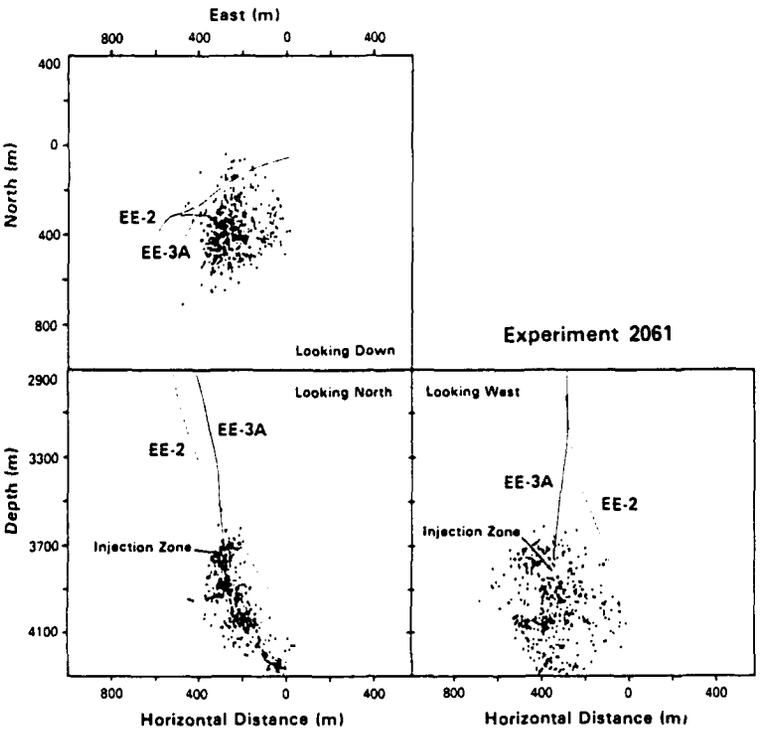

Fig. 5. Views showing locations of microseismic events accompanying experiment 2061. Views are the same as in Fig. 3. Water was injected into wellbore EE-3a in the interval labelled in the figure.

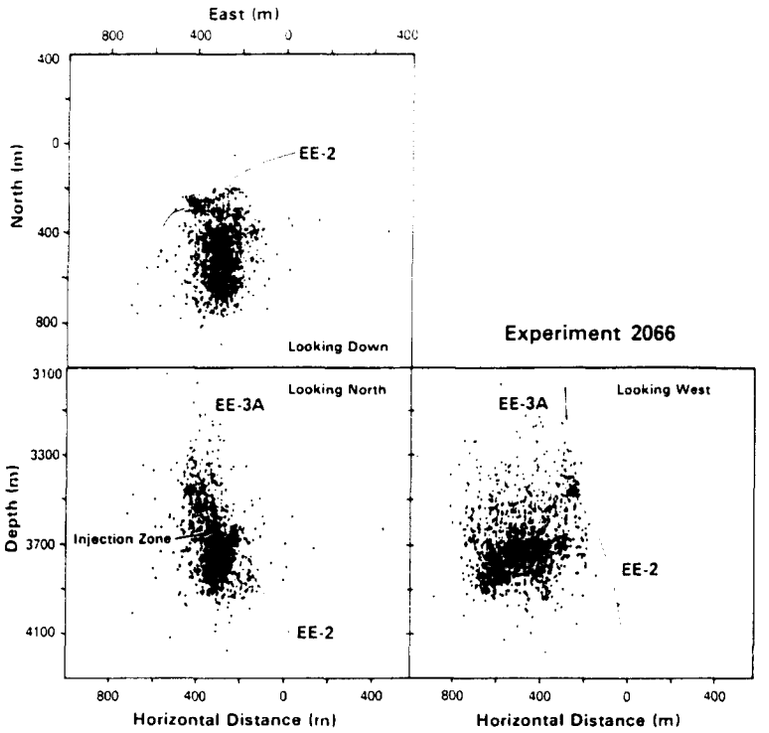

Fig. 6. Views showing locations of microseismic events accompanying experiment 2066. Views are the same as in Fig. 3. During this experiment, water was injected into wellbore EE-3a. The injection interval in labelled is the figure.

events on the plane. Maps showing locations of some of the planes found for experiment 2032 can be found in Fehler *et al.* [11].

Figure 7 shows a lower hemisphere equal area projection of the poles to the planes found by the three-point method. Symbols are used in the figure to indicate the planes as listed in Table 2. The poles define a zone trending WNW to ESE indicating that planes strike predominantly NNE. Planes striking N7°E and dipping 67°E occur in all experiments. This orientation was the first one found for experiment 2061. The azimuth of this plane is slightly different in experiment 2066, N14°E. The location of the plane is different for each experiment indicating that joints of this orientation are pervasive throughout the reservoir.

IN SITU STRESS AT FENTON HILL

Many attempts have been made to infer the state of stress at Fenton Hill. Kelkar *et al.* [21] analyzed pressure records from hydraulic injections to infer the amplitude of the least compressive stress. They assumed that the orientations of principal stresses are parallel to the *P* and *T* axes of a fault plane solution. This assumption has been shown to lead to incorrect results [22]. Dey [23] analyzed the orientations of microcracks in core re-

Table 2. Fracture planes accompanying hydraulic injections

Experiment	Plane strike	Plane dip	No. of events	Av. depth of plane (m)	Symbol in Fig. 7
2032	329	74°E	130	3383	F
2032	270	27°N	35	3738	G
2032	151	67°W	50	3165	H
2032	7	67°E	81	3548	D
2032	209	60°W	28	3594	I
2042	3	40°E	387	3728	A
2042	328	27°E	131	3513	B
2042	41	47°E	58	3511	C
2042	7	67°E	36	3754	D
2042	353	67°E	41	3517	E
2061	7	67°E	546	3930	D
2061	241	54°W	59	3766	J
2061	10	74°E	117	3913	K
2061	202	80°W	35	3570	L
2061	4	54°E	26	4103	M
2061	212	27°W	25	3721	N
2066	160	54°W	481	3760	P
2066	14	67°E	723	3701	Q
2066	119	54°W	87	3683	R
2066	153	87°W	69	3680	S

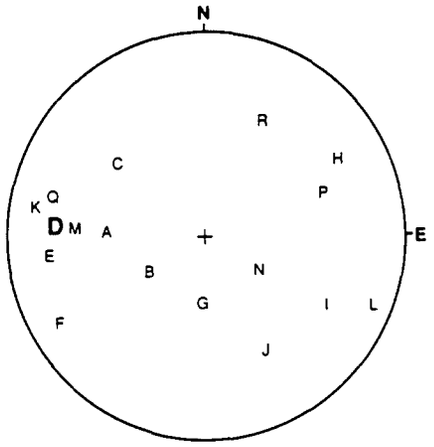

Fig. 7. Lower hemisphere equal area projection showing poles to planes found by application of the three-point method to locations accompanying four hydraulic injections. Each pole is plotted with a letter. The letters refer to the planes listed in Table 2.

moved from borehole EE-3a to determine orientations of principal stresses. He assumed that the ratio of the *in situ* stress magnitudes is proportional to the relative abundance of microcracks of each orientation. Dey [23] deduces principal stress amplitudes by assuming that the vertical stress is entirely due to the weight of the overburden. We choose not to use Dey's results because of the difficulties in determining reliable orientations of the core and the assumption that cracks in the core are a direct function of the *in situ* stress field. Barton and Zoback (written communication) analzyed borehole televiewer data to determine the orientations of wellbore breakouts measured between 3350 and 3550 m in wellbore EE-3a. Using the model of Zoback *et al.* [24] to explain the relation of wellbore breakouts to the *in situ* stress field, they concluded that the least compressive stress is horizontal and oriented N104°E. This result is in agreement with that obtained by a complete analysis of fault plane solutions of many microearthquakes by Burns (personal communication). Burns also found that the vertical stress is the maximum principle stress.

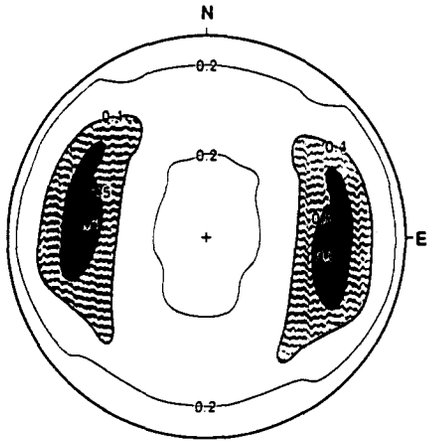

Fig. 8. Lower hemisphere equal area projections showing contours of the ratio of shear-to-normal stress acting on planes. Poles to planes are plotted. Ratios were calculated for effective stress as described in the text.

Hydraulic data taken during the phase I hot dry rock experiments, carried out at depths less than 3000 m, indicate that the ratio of effective stresses when pore pressure is only due to the hydrostatic head of water are:

$$\sigma_1/\sigma_2 = 2, \quad (1)$$

$$\sigma_2/\sigma_3 = 1.5,$$

where σ_1, σ_2 and σ_3 are the maximum, intermediate principal stresses, respectively (D. Brown, personal communication).

Although these measurements were carried out in a shallower region than that of the current work, indications are that the stress ratios are roughly comparable in the deeper region (H. Murphy, personal communication).

COMPARISON OF *IN SITU* STRESS FIELD TO ORIENTATION OF PLANES OF SLIP

McKenzie [22] has shown that knowledge of a single fault plane solution provides little constraint on the orientations of *in situ* principal stresses. Angelier [25], Gephart and Forsyth [26] and others have shown how a suite of differing fault plane solutions can be analyzed to place four constraints on the stress tensor. Unfortunately, knowing the orientation of a plane along which slip occurs places little constraint on the orientations of the principal stresses unless the direction of slip along each plane is known. We can, however, use our best estimates of the *in situ* stress tensor and infer which planes are most likely to slip.

Using the estimate of principal stress orientations given by the borehole televiewer data, and ratios of magnitudes of these stresses given in equation (1), we can calculate the ratio of shear stress acting along a given plane to the normal stress acting across the plane. For a given failure criterion, this ratio could be used to determine which planes will slip. In any event, the planes with the largest ratio of shear-to-normal stress will be those most likely to slip. The ratio of shear-to-normal stress is not simply related to any well-known failure criterion. We found, however, that the orientations of planes most likely to slip obtained by our analysis are those obtained if a Mohr–Coulomb criterion is used.

In Fig. 8, poles to planes are plotted in a lower hemisphere equal area projection and contours show regions of equal value of shear-to-normal stress acting on the plane whose pole is in a given location on the projection. There are two regions where the ratio is highest: one representing planes striking NNE and dipping east and the other striking NNE and dipping west. The poles to planes found by the three-point method fall in the regions where slip is most likely to occur. The plane with the largest ratio of shear-to-normal stress, and hence the one most likely to slip, is nearly parallel to the common plane (N7°E azimuth, dip 67°E) found in all of the experiments. The plane with the largest ratio of shear-to-normal stress is the plane most likely to slip as well as the plane along which brittle failure would

occur, should a brittle failure criterion be met. We thus cannot exclude the possibility that the planes with common orientation in all experiments represent new fractures.

Stress drops have been calculated for individual events accompanying experiment 2032 [6]. We are currently re-examining these results and have found no clear difference in stress drops between events that occurred along well-defined planes and those that did not. Thus stress drops provide no information about whether or not new fractures are being created.

Figures 3–6 show that there is a dramatic difference in the pattern of seismicity with location in the reservoir. Since different recording systems were used for the various experiments, the numbers of events located is not a good indication of the overall level of seismicity. Analogue charts recorded during the experiments showed that many more microearthquakes accompanied experiments 2042 and 2061 than 2032 and 2066. We also found that experiments 2042 and 2061 included substantially more microearthquakes that were recorded by the surface seismic network than experiments 2032 and 2066, indicating a higher total seismic energy release during experiments 2042 and 2061, since these larger events contain a majority of the energy released. The reason for the differences in seismicity between experiments is unclear but may be related to the fact that 2042 and 2061 were dominated by events occurring along one or two seismic planes, whereas the seismicity was more evenly distributed along many planes during 2032 and 2066. Perhaps the close approximity of the injection zones to planes that are oriented for slip to be favoured in experiments 2061 and 2042 caused these planes to be extremely active.

CONCLUSIONS

The three-point method has been applied to seismic data collected during four hydraulic fracturing experiments carried out at Fenton Hill, New Mexico. A suite of planes along which microearthquakes fall has been found. These planes all strike roughly NNE and dip both east and west. Since planes of many orientations were found, we must conclude that these planes were pre-existing joints in the rock that slip when the effective stress is reduced by increased pore pressure. Using best estimates of the *in situ* effective stress tensor, it is concluded that the planes found by the three-point method are those most favourably aligned for shear to occur. The orientation of the seismic plane that occurs in all experiments is the one that is predicted to have the highest ratio of shear-to-normal stress, which makes it the most likely orientation for shear slip. Presumably joints of orientations other than those found by the three-point method exist in the reservoir region but these are oriented such that shear slip is less likely to occur along them so we do not detect them.

Acknowledgements—Many people at Los Alamos contributed data and discussions that helped in performing this work. Leigh House wrote the event location scheme and assisted with data analysis. Norma McFarland picked most of the arrival times and provided consistent quality in this work. Fruitful and encouraging discussions with Schon Levy, Hugh Murphy, Don Brown, Paul Johnson, Scott Phillips, Leigh House and Kerry Burns played an important part in the formulation of the ideas in this paper. Paul Johnson, Scott Phillips, Jim Albright and Hugh Murphy assisted by critically reading the manuscript and suggesting improvements. This work was supported by the U.S. Department of Energy. Data collection was also supported by the Governments of Japan and the Federal Republic of Germany through an International Energy Agency Agreement. Computations for this work were carried out in the ESS-10 VAX computer network, which is overseen by Don Salazar, Steve Blair and Jim Krone. Their efforts at providing a superb computation facility is greatly appreciated.

REFERENCES

1. Albright J. N. and Hanold R. L. Seismic mapping of hydraulic fractures made in basement rocks. *Proc. 2nd ERDA Enhanced Oil and Gas Recovery Symp.* (1976).
2. Albright J. N. and Pearson C. Acoustic emissions as a tool for hydraulic fracture locations: experience at the Fenton Hill hot dry rock site. *Soc. Petro. Engrs J.* 523–530 (1983).
3. Pearson C. Source parameters and a magnitude moment relationship from small local earthquakes observed during hydraulic fracturing experiments in crystalline rock. *Geophys Res. Letts* **9**, 404–407 (1982).
4. Keppler H., Pearson C., Potter R. and Albright J. Microearthquakes induced during hydraulic fracturing at the Fenton Hill HDR site: the 1982 experiments. *Trans. Geothermal Resources Council*, 7, 429–433. (1983).
5. House L., Keppler H. and Kaieda H. Seismic studies of a massive hydraulic fracturing experiment. *Trans. Geotherm. Res. Council* **9**, (part II), 105–110 (1985).
6. Fehler M. and Bame D. Characteristics of microearthquakes accompanying hydraulic fracturing as determined from studies of spectra of seismic waveforms. *Trans. Geotherm. Res. Council* **9** (part II), 11–16 (1985).
7. Pearson C. The relationship between microseismicity and high pore pressure during hydraulic stimulation experiments in low permeability granite rocks. *J. Geophys* **86**, 7855–7864 (1981).
8. Murphy H. and Fehler M. Hydraulic fracturing of jointed formations. *Soc. Petrol. Engrs, Int. Mg Petrol. Engng*, March 17–20, Beijing, China. SPE, Paper 14088 (1986).
9. Cash D., Homuth E., Keppler H. Pearson C. and Sasaki S. Fault plane solutions for microearthquakes induced at the Fenton Hill hot dry rock geothermal site: implications for the state of stress near a quaternary volcanic center. *Geophys Res. Letts* **10**, 1141–1144 (1983).
10. Kaieda H. Hypocenter distribution and fault plane solutions of microearthquakes induced by hydraulic fracturing as determined by observations from a surface seismic network. *EOS Trans. Am. geophys Un.* **65**, 1011 (1984).
11. Fehler M., House L. and Kaieda H. Determining planes along which earthquakes occur: method and application to earthquakes accompanying hydraulic fracturing. *J. Geophys Res.* **92**, 9407–9414 (1987).
12. Bame D. and Fehler M. Observations of long period earthquakes accompanying hydraulic fracturing. *Geophys Res. Letts* **13**, 149–152 (1986).
13. Majer E. and Doe T. Studying hydrofractures by high frequency seismic monitoring. *Int. J. Rock Mech. Min Sci & Geomech. Abstr.* **23**, 185–199 (1986).
14. Ferrazzini V., Aki K., Chouet B. and Fehler M. Very slow waves trapped in a fluid layer sandwiched between two solid half spaces with application to the long period-period earthquakes. *EOS Trans. Am. geophys. Un.* **67**, 1203 (1986).
15. Fehler M. and Chouet B. Operation of a digital seismic network on Mt St Helens volcano and observations of long period seismic events that originate under the volcano. *Geophys Res. Lett.* **9**, 1017–1020 (1986).
16. Cundall P. and Marti J. Computer modeling of jointed rock masses. Report N-78-4, U.S. Army Corps of Engineers, Waterways Experiment Station, Vicksburg, Miss. (1978).
17. Brown S. R. Fluid flow through rock joints: the effect of surface roughness. *J. Geophys Res.* **92**, 1337–1347 (1987).

18. House L. Locating microearthquakes induced by hydraulic fracturing in crystalline rock. *Geophys Res. Letts* **14**, 919–921 (1987).
19. Lutz T. An analysis of the orientations of large-scale crystal structures: a statistical approach based on areal distributions of pointlike features. *J. Geophys Res.* **91**, 421–434 (1986).
20. Pine R. and Batchelor A. Downward migration of shearing in jointed rock during hydraulic injection. *Int. J. Rock Mech. Min. Sci. Geomech. Abstr.* **21**, 249–263 (1984).
21. Kelkar S., Murphy H. and Dash Z. Earth stress measurements in deep granitic rock. Rock mech. key to energy production. *Proc. 27 U.S. Symp. Rock Mech.*, Society of Mining Engrs, pp. 259–266, (1986).
22. McKenzie D. The relation between fault plane solutions for earthquakes and the directions of the principal stresses. *J. Geophys Res.* **59**, 591–601 (1969).
23. Dey T. Stress measurements in a deep granitic rock mass near Valles Caldera at Fenton Hill, New Mexico (presentation) (1987).
24. Zoback M., Moos D. and Mastin L. Well bore breakouts and *in situ* stress. *J. Geophys Res.* **90**, 5523–5530 (1985).
25. Angelier J. Determination of the mean principal stress directions for a given fault population. *Tectonophysics* **56**, T17–T26 (1979).
26. Gephart J. and Forsyth D. An improved method for determining the regional stress tensor using earthquake focal mechanism data: application to the San Fernando earthquake sequence. *J. Geophys Res.* **89**, 9305–9320 (1984).